Journal of Electroanalytical Chemistry 767 (2016) 153–159

Contents lists available at ScienceDirect

Journal of Electroanalytical Chemistry

journal homepage: www.elsevier.com/locate/jelechem

Evaluation of the kinetic parameters of the hydrogen oxidation reaction on nanostructured iridium electrodes in alkaline solution

María A. Montero, María R. Gennero de Chialvo, Abel C. Chialvo *

Programa de Electroquímica Aplicada e Ingeniería Electroquímica (PRELINE), Facultad de Ingeniería Química, Universidad Nacional del Litoral, Santiago del Estero 2829, 3000, Santa Fe, Argentina

ARTICLE INFO

Article history:
Received 5 January 2016
Received in revised form 12 February 2016
Accepted 14 February 2016
Available online 18 February 2016

Keywords:
Hydrogen oxidation
Nanostructured iridium
Alkaline solution

ABSTRACT

The kinetic study of the hydrogen oxidation reaction on a nanostructured iridium electrode was carried out in alkaline solution at different rotation rates. The electrode, prepared by sputtering on a glassy carbon substrate, was characterized by cyclic voltammetry, AFM and XPS techniques. Then, the experimental current density (j) vs. overpotential (η) curves were recorded in the range comprised between $-0.015 \le \eta\,/\mathrm{V} \le 0.30$. The correlation of the resulting curves was carried out considering the Tafel-Heyrovsky-Volmer mechanism, with a Frumkin type isotherm for the adsorption of the reaction intermediate. The kinetic parameters (equilibrium reaction rates of the elementary steps and surface coverage of the adsorbed hydrogen) were evaluated. The results obtained indicate that, in the potential range evaluated, the reaction takes place mainly through the Tafel-Volmer route with a small contribution of the Heyrovsky-Volmer route. Finally, an explanation for the lower electrocatalytic activity observed in alkaline solutions with respect to that in acid solutions was proposed, on the basis of the movement restrictions of the hydroxyl ion inside the superficial water network to make possible the electron transference in the Volmer and Heyrovsky steps.

1. Introduction

The alkaline membrane fuel cells (AMFCs) show potential advantages over the proton exchange membrane fuel cells (PEMFCs), such as the greater reaction rate of the oxygen reduction reaction, which make their development highly attractive [1]. This fact has promoted the study of the electrodic reactions involved in this type of fuel cells. However, publications related to the kinetic analysis of the hydrogen oxidation reaction (hor) in alkaline solutions are relatively scarce [2–8]. It is usually considered that the reaction rate of the hor in alkaline solutions is significantly less than that in acid solutions [3,5,6]. This statement is based in the comparison of the exchange current density (j°), which values are one [5] to two [6] orders of magnitude lower in alkaline than in acidic media. However, the experimental evaluation of this kinetic parameter is usually carried out with many approximations and assumptions, which lead to uncertainties in the conclusions. A more rigorous kinetic treatment, involving the simultaneous occurrence of the three steps of the Tafel-Heyrovsky-Volmer mechanism on steady state, was developed by our group [9,10]. The correlation of the $j(\eta)$ curves with the theoretical equations allows the calculation of the elementary kinetic parameters (equilibrium reaction rates of each step, equilibrium surface coverage of the adsorbed hydrogen, etc.). On this basis, the reaction is described in absence of kinetic approximations and then, the value of j° can be calculated from a given set of the elementary kinetic parameters. Thus, it was recently carried out for the first time the kinetic study of the hor on nanostructured rhodium electrodes in acid [11] and alkaline [8] solutions. The results obtained showed that in both cases the reaction takes place preferably through the Tafel-Volmer route, with a small contribution of the Heyrovsky-Volmer route. The comparison of the corresponding values obtained for j° indicated that it is less than one order of magnitude lower in alkaline solution than in acid solution. Such decrease in the electrocatalytic activity was ascribed to the role played by the water molecules network located on the electrode surface [8]. In this context and taking into account that a kinetic study of the hydrogen oxidation reaction on a nanostructured iridium electrode in acid solution was already carried out [12], the present work deals with the evaluation of the kinetic parameters of the hor on this electrode material in alkaline solution, which can provide further evidence of the role of the water network on the reaction kinetics.

2. Materials and methods

2.1. Electrochemical measurements

Electrochemical experiments were performed in a three-electrode cell specially built for the use of a rotating electrode and with a particular design of the gas saturator at 25 °C, in order to ensure constant

* Corresponding author.
E-mail address: achialvo@fiq.unl.edu.ar (A.C. Chialvo).

http://dx.doi.org/10.1016/j.jelechem.2016.02.024
1572-6657/

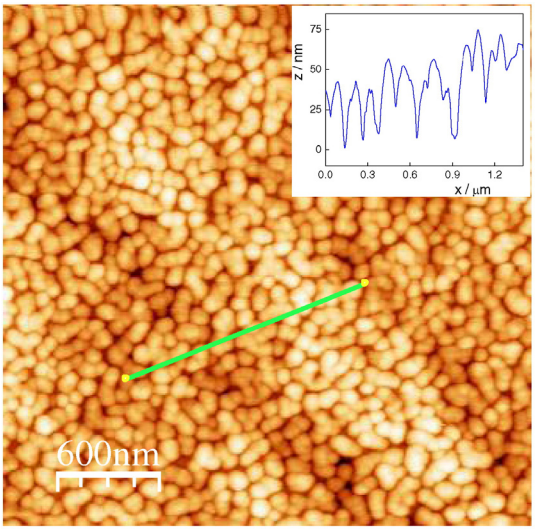

Fig. 1. Micrograph of nanostructured iridium obtained by AFM. Inset: height profile.

hydrogen saturation during experiments without affecting the fluid dynamics of the solution near the electrode. The counterelectrode was a platinum helical wire of large area, located in an external compartment in order to avoid contamination of the working electrode. Measurements were carried out in a 0.1 M NaOH solution prepared with ultrapure water, with the exception of the solution employed for the electrode area determination, which was 0.5 M H_2SO_4. The nanostructured iridium was prepared via sputtering on a glassy carbon substrate from an Ir target and the details are given elsewhere [12]. Then, the working electrode, with an exposed geometric area of 0.167 cm^2, was mounted in a teflon holder which can be rotated at different rotation rates. The Luggin capillary of 0.2 mm diameter, located at 0.2 mm of the electrode surface, ensures a negligible ohmic effect on the experimental conditions and does not affect the fluid dynamics of the solution. Potentials were measured in both, alkaline and acid media, against a hydrogen electrode (RHE) immersed in the same solution. The electrode was characterized by cyclic voltammetry in a nitrogen saturated solution,

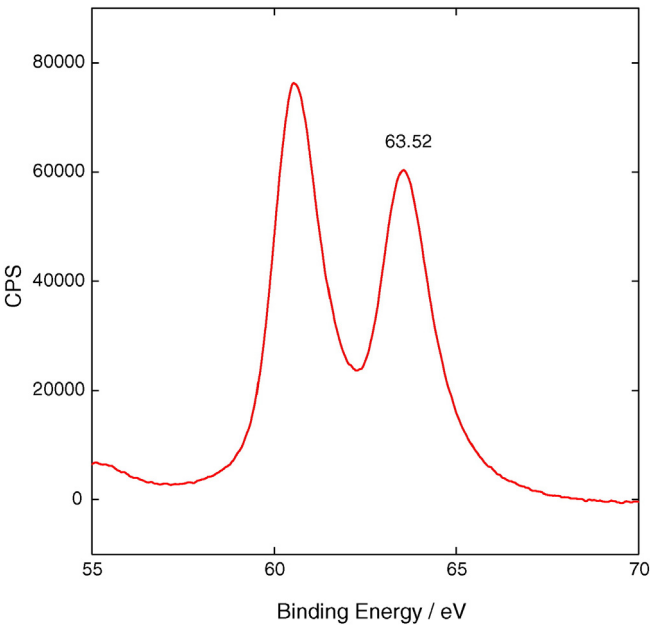

Fig. 2. XPS spectra of nanostructured iridium.

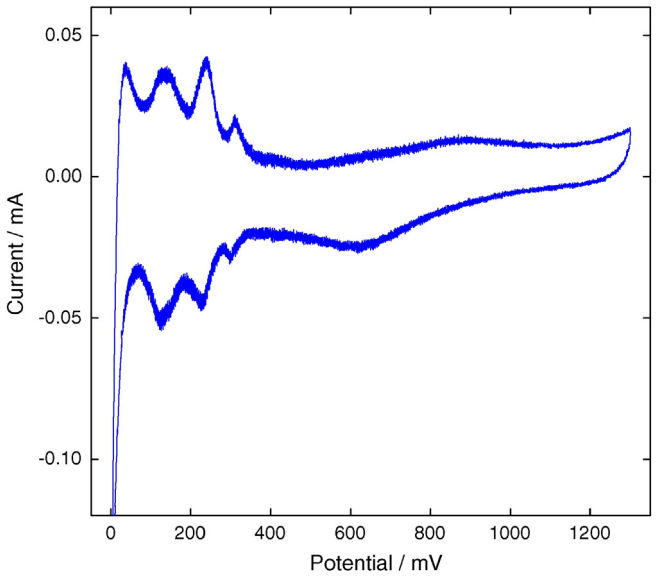

Fig. 3. Voltammetric profile of the Ir electrode in 0.1 M NaOH at 0.05 V s^{-1} and 25 °C.

at a sweep rate of 0.1 V s^{-1} between 0.0 and 1.3 V. Before the measurement of the current - potential dependence corresponding to the hydrogen oxidation, it was verified that the Ir electrode reached the equilibrium potential of the hydrogen electrode reaction, as well as the absence of absorbed hydrogen inside iridium metal. In order to confirm these conditions, the variation of the open circuit potential with time was recorded under hydrogen saturation from both, an anodic and a cathodic potential with respect to equilibrium.

2.2. Electrode characterization

The surface morphology of the working electrode was characterized by Atomic Force Microscopy (AFM) and X-ray Photoelectron spectroscopy (XPS). AFM images were obtained using an Agilent microscope 5400, operated in tapping mode and processed with the software WSxM 6.2. XPS analysis was carried out with a multitechnique system

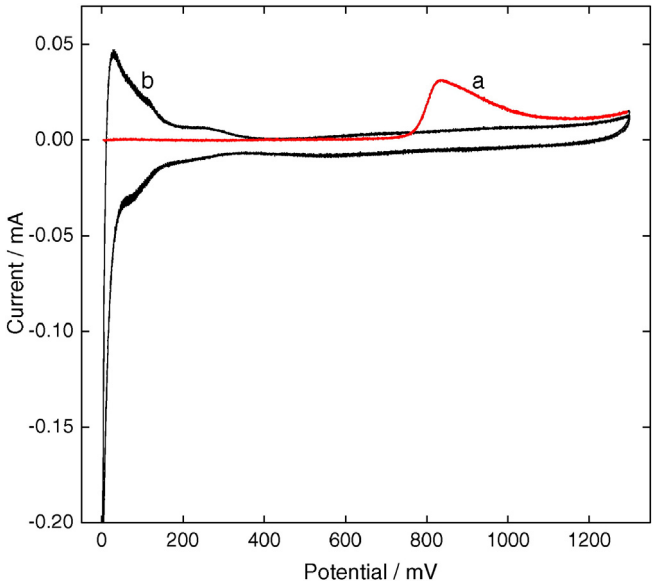

Fig. 4. Voltammetric stripping of adsorbed CO on the Ir electrode. (a) First cycle; (b) Second cycle. 0.05 V s^{-1}; 0.5 M H_2SO_4, 25 °C.

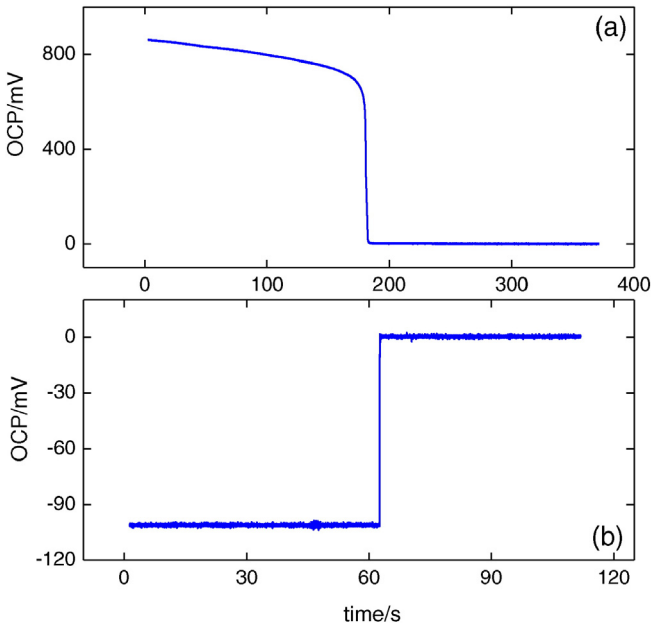

Fig. 5. Open circuit potential vs. time response of the Ir electrode after polarization at (a) 0.9 V; (b) -0.1 V. 0.1 M NaOH; 25 °C.

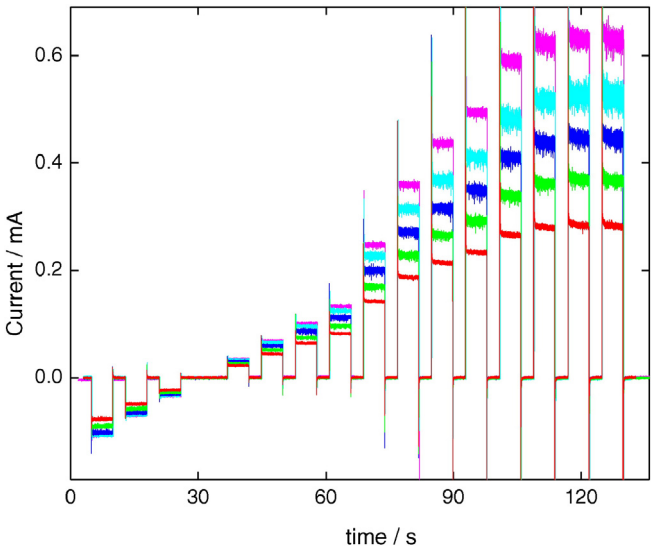

Fig. 6. Current vs. time response of Ir electrode to the program applied in the range $-0.015\ V \le \eta \le 0.30\ V$ at rotation rates $\omega = 900$; 1600; 2500; 3600 and 4900 rpm. 0.1 M NaOH; 25 °C.

equipment (SPECS). The spectra was obtained in the spectral region corresponding to the Ir 4f core level, with pass energy of 30 eV, the MgKa X-ray source operated at 200 W - 12 kV and a working pressure less than 5.9 10^{-7} Pa.

2.3. Evaluation of the current-overpotential dependence

The hydrogen oxidation reaction was studied through the current (I) - overpotential (η) response in hydrogen saturated solution at 25 °C. The polarization curves were obtained at different rotation rates in the range $900 \le \omega/\text{rpm} \le 4900$. A potential program was applied, which consisted in a 3 s step at 0.0 V, followed by a 5 s step to a given overpotential value. In this last period, readings of the current value were made each 0.01 s. Then the program was repeated for each η value, which was varied in the range $-0.015 \le \eta/\text{V} \le 0.30$. The electrolyte solution was renewed after each experiment.

Finally, the real area of the electrode was determined by CO stripping voltammetry. This evaluation was carried out in an auxiliary cell in a 0.5 M H_2SO_4 solution saturated with CO, holding the electrode potential at 0.05 V during 15 min. After the CO removal by nitrogen bubbling, the voltammetric stripping was applied at 0.05 V s^{-1} between 0.0 V and 1.3 V. An important aspect that should be emphasized is that repetitive potential cycling was avoided because it develops an oxide redox couple which denaturalizes the electrode surface. Thus, a unique potentiodynamic sweep was applied in order to characterize the working electrode.

3. Results and discussion

3.1. Surface characterization

The image of the surface morphology obtained by AFM is illustrated in Fig. 1. It can be observed that the Ir layer, deposited by sputtering on a glassy carbon substrate, consists of uniformly distributed nanoparticles. In order to estimate the particle size, the height profile was analyzed in different locations on the electrode surface. One of them is illustrated in the inset of Fig. 1. The average height of the nanoparticles obtained from these profiles is ranging between 15 to 30 nm. On the other hand, Fig. 2 shows the XPS spectrum in the range of binding energy comprised 55 and 75 eV. Two peaks located at 60.58 and 63.52 eV respectively can be observed that correspond to the $4f_{7/2}$ and $4f_{5/2}$ binding energy of metallic iridium [13–15] and, in agreement with the electrochemical evidences, the contribution of the oxide species can be considered negligible.

3.2. Electrochemical characterization and real area evaluation

Fig. 3 shows the voltammetric profile of the Ir electrode obtained in 0.1 M NaOH solution between 0.0 and 1.30 V at 0.05 Vs^{-1}, which is similar to that already described in the literature [16]. It can be appreciated the three reversible peaks corresponding to the adsorption/desorption of the underpotentially deposited hydrogen (H_{UPD}) in the range comprised between 0.05 and 0.4 V. Then, the irreversible couple ascribed to the adsorption/desorption of oxygen can be identified by a small anodic peak at 0.9 V and the corresponding cathodic peak at 0.6 V. It should be taken into account that the presence of an oxide layer on the electrode surface is evidenced through a couple of highly symmetric voltammetric peaks, anodic and cathodic respectively, near 0.6 V [16]. This response, characteristic of the Ir oxide electrode, is not observed in Fig. 3, verifying the result obtained in the XPS spectrum related to the negligible amount of oxide over the surface.

The electrode area was evaluated from the charge resulting from the anodic stripping of the adsorbed CO, method already employed in the study of the hor on Ir in acid solution [12]. From the voltammetric response of the CO stripping, shown in Fig. 4, the value of the charge involved in the CO oxidation was 101 μC. Taking into account that the charge of a monolayer is 287.7 μC cm^{-2} (discussed in detail in [12]), an area of 0.35 cm^2 was obtained. Moreover, the resulting value of the active area factor (relationship between real and geometric area) is $f_{aa} = 2.1$. This relationship is an

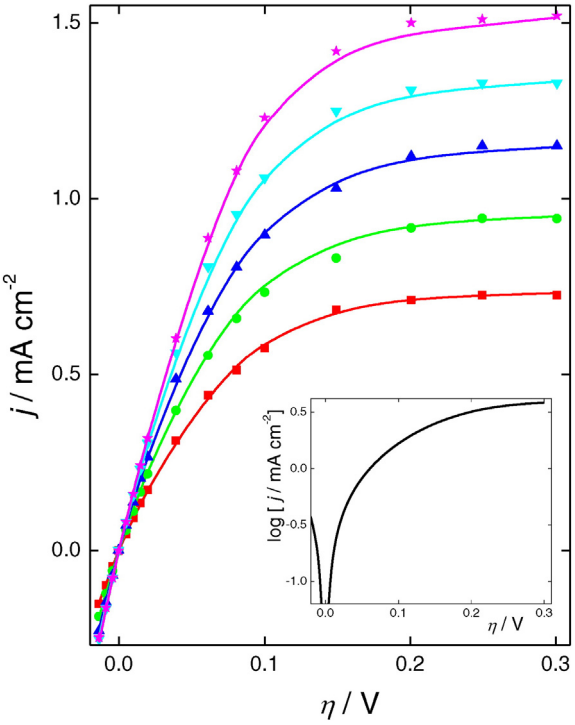

Fig. 7. Experimental (symbols) and simulated (lines) $j(\eta)$ curves of the hor on the Ir electrode. 0.1 M NaOH; 25 °C $\omega =$ (■) 900; (●) 1600; (▲) 2500; (▼) 3600; (★) 4900 rpm. Inset: Polarization plot in absence of mass transfer contribution.

important parameter for the correct analysis of the reaction under study because the hor has a strong diffusion contribution, which depends on the geometric area, meanwhile the kinetic reaction depends on the real surface area.

3.3. Verification of the equilibrium potential

The evaluation of the electrocatalytic activity of the Ir electrode was carried out including potential values surrounding the equilibrium potential. Therefore, it was important to verify that such condition was achieved. This verification was performed by polarization of the electrode at 0.9 V vs. RHE during 30 s and then the circuit was open and the dependence of the open circuit potential on time was recorded. This dependence is illustrated in Fig. 5a. It can be appreciated that oxygen electroadsorbed at 0.9 V was reduced by the molecular hydrogen and finally the potential fell to the reversible equilibrium value (0.0 V). Then the electrode was polarized cathodically (− 0.1 V). When the electric circuit was opened, potential increased and immediately reached equilibrium, as it can be observed in Fig. 5b. This state was maintained when measurements were carried out at potential values in the range comprised between −0.1 V and 0.5 V. These results demonstrate that the behaviour of the interphase Ir/alkaline solution in the presence of molecular hydrogen is governed by the hydrogen electrode reaction.

3.4. Experimental current-overpotential dependence

The evaluation of the experimental dependence I vs. η for the hydrogen oxidation reaction on a nanostructured Ir electrode was carried out in 0.1 M NaOH solution under hydrogen bubbling at different rotation rates ($900 \le \omega/\text{rpm} \le 4900$). After the open circuit potential reached the equilibrium value (0.0 ± 0.0004 V vs. RHE), the potential program was applied for all the rotation rates analyzed (900, 1600, 2500, 3600 and 4900 rpm). It can be observed that the electrode current on time quickly reached the steady state condition (Fig. 6). The mean value of the current data measured in the last 2 s was assigned to the step overpotential and then, taking into account the real electrode area, the corresponding $j^{exp}(\eta)$ dependences on steady state were evaluated for each rotation rate, which are shown in Fig. 7 (symbols).

Furthermore, in order to obtain the elementary kinetic parameters, a model that describes theoretically the dependence $j(\eta)$ is necessary, which is described in the next item.

3.5. Kinetic model for the description of the hydrogen oxidation reaction

The hydrogen oxidation reaction on noble metals is described by the Tafel-Heyrovsky-Volmer (THV) mechanism, which steps can be written in alkaline solution as follows [8].

$$H_2 + 2S \rightleftarrows 2H_{ad} \quad Tafel \tag{1.a}$$

$$H_2 + OH^- + S \rightleftarrows H_{ad} + H_2O + e^- \quad Heyrovsky \tag{1.b}$$

$$H_{ad} + OH^- \rightleftarrows H_2O + e^- + S \quad Volmer \tag{1.c}$$

where S is an active site on which the reaction intermediate H_{ad} can be adsorbed. The interpretation of the experimental dependence $j^{exp}(\eta)$ needs the resolution of the reaction mechanism, which was carried out previously without kinetic approximations and considering that the adsorbed intermediate follows a Frumkin type adsorption isotherm [9].

Thus, the current density referred to the real area is described by the following equation

$$j = \frac{v_H^e e^{-u(\theta-\theta^e)\lambda} e^{\alpha_H f\eta}\left[\frac{(1-\theta)}{(1-\theta^e)} - \frac{\theta e^{-f\eta} e^{u(\theta-\theta^e)}}{\theta^e}\right] + v_T^e e^{-2u(\theta-\theta^e)\lambda}\left[\frac{(1-\theta)^2}{(1-\theta^e)^2} - \frac{\theta^2 e^{2u(\theta-\theta^e)}}{\theta^{e2}}\right]}{\frac{1}{2F} + \frac{v_T^e f_{aa}(1-\theta)^2 e^{-2u(\theta-\theta^e)\lambda}}{B\omega^{1/2}(1-\theta^e)^2} + \frac{v_H^e f_{aa}(1-\theta) e^{-u(\theta-\theta^e)\lambda} e^{\alpha_H f\eta}}{B\omega^{1/2}(1-\theta^e)}} \tag{2}$$

where v_i is the reaction rate of the step i (i = T, H, V), λ is the symmetry factor of adsorption, u (in RT units) is the energy of interaction between the adsorbed hydrogen atoms, α_i (i = V,H) is the symmetry factor of the step i and B is the constant of the Levich equation, $j_L = B\omega^{1/2}$, where j_L represents the limiting diffusion current density referred to the diffusion section (geometric area). Finally, the equilibrium condition is indicated by the superscript e and $f = F/RT$. The variation of the surface coverage of the adsorbed hydrogen on overpotential and on the rotation rate is described by the following implicit equation, $g(\theta,\eta,\omega) = 0$ [9]

$$\begin{aligned}
&\left\{v_V^e e^{-u(\theta-\theta^e)\lambda} e^{\alpha_V f\eta}\left[\frac{\theta e^{u(\theta-\theta^e)}}{\theta^e} - \frac{(1-\theta)e^{-f\eta}}{(1-\theta^e)}\right] + v_H^e e^{-u(\theta-\theta^e)\lambda} e^{\alpha_H f\eta}\left[\frac{(1-\theta)}{(1-\theta^e)} - \frac{\theta e^{-f\eta} e^{u(\theta-\theta^e)}}{\theta^e}\right]\right\}\times \\
&\left\{\frac{1}{2F} + \frac{v_T^e f_{aa}(1-\theta)^2 e^{-2u(\theta-\theta^e)\lambda}}{B\omega^{1/2}(1-\theta^e)^2}\right\} - \left\{\frac{1}{F} + \frac{v_H^e f_{aa}(1-\theta) e^{-u(\theta-\theta^e)\lambda} e^{\alpha_H f\eta}}{B\omega^{1/2}(1-\theta^e)}\right\}\times \\
&\left\{v_V^e e^{-u(\theta-\theta^e)\lambda} e^{\alpha_V f\eta}\left[\frac{\theta e^{u(\theta-\theta^e)}}{\theta^e} - \frac{(1-\theta)e^{-f\eta}}{(1-\theta^e)}\right] - v_T^e e^{-2u(\theta-\theta^e)\lambda}\left[\frac{(1-\theta)^2}{(1-\theta^e)^2} - \frac{\theta^2 e^{2u(\theta-\theta^e)}}{\theta^{e2}}\right]\right\} = 0
\end{aligned} \tag{3}$$

The analysis of Eqs. (2) and (3) leads to important conclusions that are necessary for the correct evaluation of the kinetic parameters of the hor. At first, it was demonstrated that these equations predict a transition between the Tafel- Volmer (TV) route, which prevails at lower overpotentials, and the Heyrovsky-Volmer (HV) route, more relevant at higher overpotentials [17]. If such transition is verified at high values (η > 0.40 V), a current density plateau is achieved before the transition, which is called $j_{max}(\omega)$. This is always lower than $j_L(\omega)$ and is given by the following expression [9,12]

$$\frac{1}{j_{max}(\omega)} = \frac{1}{j_{max}^{kin}} + \left(\frac{f_{aa}}{B}\right)\frac{1}{\omega^{1/2}} \tag{4}$$

where $j_{max}{}^{kin}$ is the limiting kinetic current density of the Tafel step, which is defines as follows [9,12]

$$j_{max}^{kin} = \frac{2Fv_T^e e^{2\lambda u\theta^e}}{(1-\theta^e)^2} \tag{5}$$

It should be noticed that Eq. (4), although resembles the Koutecky-Levich expression, is valid only in the overpotentials region previously described [9,10]. Moreover, Eq. (5) will be used in the evaluation of the kinetic parameters described in the next item.

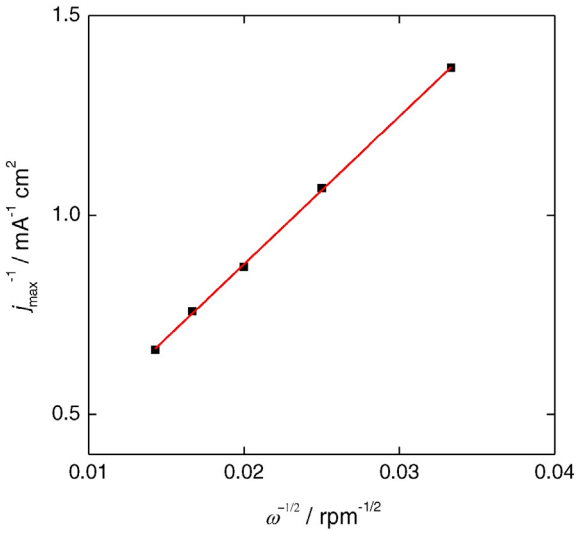

Fig. 8. j_{max}^{-1} vs. $\omega^{-1/2}$ plot. Experimental (symbols), linear regression (line).

Table 1
Kinetic parameters of the hor obtained from the correlation of the experimental curves.

Kinetic Parameters	Rotation rate/rpm					Mean Value
	900	1600	2500	3600	4900	
$v_T^e \times 10^9$/mol cm^{-2} s^{-1}	1.85 ± 1.09	1.51 ± 0.33	1.99 ± 0.60	1.98 ± 0.32	2.29 ± 0.61	1.92 ± 0.25
v_H^e /mol cm^{-2} s^{-1}	$<10^{-17}$	$<10^{-17}$	$<10^{-17}$	$<10^{-17}$	$<10^{-17}$	$<10^{-17}$
$v_V^e \times 10^9$/mol cm^{-2} s^{-1}	4.71 ± 2.45	9.00 ± 4.17	9.00 ± 6.32	20.0 ± 6.94	19.9 ± 11.7	12.5 ± 6.26
θ^e	0.369 ± 0.186	0.368 ± 0.071	0.370 ± 0.096	0.375 ± 0.051	0.375 ± 0.084	0.371 ± 0.003
u	5.71 ± 2.66	6.3 ± 2.17	5.5 ± 2.5	5.39 ± 1.34	5.0 ± 2.16	5.58 ± 0.42

3.6. Evaluation of the kinetic parameters

The experimental data shown in Fig. 7 were correlated with the system of Eqs. (2) and (3). Moreover, the value of the constant B was calculated from Eq. (4). It can be observed that the plot j_{max}^{-1} vs. $\omega^{-1/2}$ (Fig. 8) satisfies the required linearity of this equation. The values obtained from slope and origin ordinate respectively are $f_{aa}/B = 37.073\ \text{mA}^{-1}\ \text{cm}^2\ \text{rpm}^{1/2}$ and $(j_{\max}{}^{kin})^{-1} = 0.135\ \text{mA}^{-1}\ \text{cm}^2$. From this result and taking into account Eq. (5), the following relationship between the parameters v_T^e and θ^e is obtained

$$v_T^e\left[\text{mol cm}^{-2}\text{s}^{-1}\right] = 3.838\,10^{-8}\left(1-\theta^e\right)^2 e^{-2\lambda u\theta^e} \tag{6}$$

A non linear least squares regression method was applied for the correlation of the experimental $j(\eta,\omega)$, which was carried out with the software Micromath Scientist 3.0. For the symmetry factors α_V, α_H and λ the value of 0.5 were assigned. The kinetic parameters v_H^e, v_V^e, θ^e and u were evaluated from the correlation and the value of v_T^e was obtained from Eq. (6). Each experimental dependence $j(\eta, \omega)$ was correlated independently for the different rotation rates and the resulting values of the kinetic parameters are shown in Table 1 and illustrated in Fig. 7 as lines. It can be appreciated that there is a good agreement between the experimental and simulated curves and that in the analyzed potential range the hydrogen oxidation is basically verified through the Tafel-Volmer route, meanwhile the Heyrovsky-Volmer route can be considered negligible in the range of overpotentials under analysis.

On the other hand, starting from the set of kinetic parameters, the activated or kinetic dependence $j(\eta)$, that is in absence of mass transfer contributions, can be also obtained. It was simulated by cancelling in Eqs. (2) and (3) the terms containing the rotation rate (equivalent to make $j_L \to \infty$). The resulting curve, plotted as log j vs. η, is illustrated in the inset of Fig. 7.

3.7. Electrocatalytic activity

The electrocatalytic activity of a given electrode material for the hydrogen electrode reaction is generally represented by the exchange current density (j^o), which is related to the kinetic parameters by the following equation [11,12],

$$j^o = 2F\left(\frac{v_T^e v_V^e + v_H^e v_V^e + v_T^e v_H^e}{\left(v_V^e + v_H^e + 2v_T^e\right)}\right) \tag{7}$$

The value obtained from the data given in Table 1 was 0.2846 mA cm^{-2}, less than the value (1.34 mA cm^{-2}) evaluated in acid solution [12]. Moreover, the equilibrium polarization resistance (R_p^o) can be also evaluated from the kinetic parameters [11,12],

$$R_p^o = \frac{RT}{4F^2}\left(\frac{4v_T^e + v_H^e + v_V^e}{v_T^e v_V^e + v_H^e v_V^e + v_T^e v_H^e}\right) \tag{8}$$

The resulting value is $R_p^o = 55.349\ \Omega\ \text{cm}^2$, which is higher than that observed in acid media (9.62 Ω cm^2) [12].

The lower value of the electrocatalytic activity of the hor in alkaline solution with respect to that on acid solutions has been interpreted on terms of the electroadsorption of hydroxyl ions [5,17]:

$$OH^- + S \rightleftarrows OH_{ad} + e^- \tag{9}$$

Reaction (9) would inhibit the sites (S) for the adsorption of H_{ad}. This process should produce a sigmoid type dependence for the OH_{ad} surface coverage on overpotential [18–20]. It would go along with a decrease of current density [19,20]. However, this behaviour was not observed in the overpotential range under study, where a current plateau is obtained. The expected behaviour should be similar to that found on Ru [19] and Pt [20] in acid solution, due to water electroadsorption, although at lower potentials. Therefore, the hydroxyl electroadsorption should be discarded as the responsible for the decrease in the electrocatalytic activity in alkaline solution. Consequently, an interpretation based on the differences between the elementary reaction steps (T, H, V) in both media will be considered here. The reaction mechanism in acid is as follows,

$$H_2 + 2S \rightleftarrows 2H_{ad} \tag{1.a}$$

$$H_2 + S \rightleftarrows H_{ad} + H^+ + e^- \tag{10.b}$$

$$H_{ad} \rightleftarrows H^+ + e^- + S \tag{10.c}$$

The Tafel step, reaction (1.a), is the same in alkaline and acid solutions, but Heyrovsky and Volmer steps involve different species, as it follows from the comparison of reactions (10.b) and (10.c) with (1.b) and (1.c) respectively. This implies, from a kinetic point of view, a marked difference in the formation and breaking of the chemical bonds. Thus, the different species involved in the elementary steps (H^+ in acid, OH^- and H_2O in alkaline) lead to differences in the corresponding potential free energy surfaces [21]. As a result, differences in the activation free energies of these steps in both media can be expected and therefore in the corresponding equilibrium reaction rates. On the contrary, the v_T^e values should be similar in alkaline and acid solutions. This statement can be verified from the values obtained for Ir electrodes in this study, $v_T^e]_{alk} = 2.02\ 10^{-9}$ mol s^{-1} cm^{-2}, and from previous results [12], $v_T^e]_{ac} = 6.92\ 10^{-9}$ mol s^{-1} cm^{-2}. Moreover, similar results were obtained on Rh electrodes, where the values of the equilibrium reaction rate of the Tafel step were $v_T^e]_{alk} = 1.128\ 10^{-9}$ mol s^{-1} cm^{-2} [8] and $v_T^e]_{ac} = 1.257\ 10^{-9}$ mol s^{-1} cm^{-2} [11].

With respect to the values of the equilibrium reaction rates of the Heyrovsky and Volmer steps, it is straightforward that they should be different for alkaline and acid solutions, but the lower values in alkaline must be explained. This can be done on the basis of the behaviour of the species involved in the reactions. In acid solutions, in both steps proton is incorporated in the water network as electron is transferred to the metallic substrate. Meanwhile, in alkaline solution the electron transference goes along with the disappearance of a hydroxyl ion. It should be noticed that both species enter or leave the reaction plane by a Grotthuss type mechanism, which implies the transfer of hydrogen bonds through a highly ordered water network. In this context, it is evident that it is more difficult for OH^- than for H^+ to achieve the appropriate spatial configuration to enable the electron transference in the constrains of the surface water network. This fact implies an increase of the activation energies of the Heyrovsky and Volmer steps in alkaline solution and therefore a decrease of the corresponding equilibrium reaction rates, which is in agreement with the results obtained for the two electrodes studied, iridium and rhodium. The corresponding values on Ir for the Volmer step are: $v_V^e]_{alk} = 1.19\ 10^{-8}$ mol s^{-1} cm^{-2} (present study) and $v_V^e]_{ac} = 9.89\ 10^{-5}$ mol s^{-1} cm^{-2} [12]. Meanwhile, the results obtained on Rh electrodes were $v_V^e]_{alk} = 2.67\ 10^{-9}$ mol s^{-1} cm^{-2} [8] and $v_V^e]_{ac} = 5.54\ 10^{-8}$ mol s^{-1} cm^{-2} [11]. It should be important to note that the nature of the metallic substrate influences the interaction of the species with the water network and with the adsorbed intermediate and therefore it can be expected differences between the values obtained for both electrodes. In the case of the Heyrovsky step, although a similar behaviour is observed, its contribution to the hydrogen oxidation reaction is less significant in the range of overpotentials under study, where Tafel-Volmer is the prevailing route.

4. Conclusions

The kinetic study of the hydrogen oxidation reaction on a nanostructured iridium electrode in alkaline solution was carried out. The polarization curves on steady state were recorded at different rotation rates and then they were correlated with kinetic equations derived for the Tafel-Heyrovsky-Volmer mechanism, allowing the evaluation of the equilibrium reaction rates of the elementary steps, which were compared with previous values obtained in acid solution. From this comparison as well as of those corresponding to rhodium in both media, an interpretation for the lower value of the electrocatalytic activity of the hor in alkaline solution with respect to acid solution was given. This is mainly based on the constraints of the hydroxyl ion inside the superficial water network to make possible the electron transference in the Volmer and Heyrovsky steps.

Acknowledgements

The authors wish to acknowledge the financial support received from ANPCyT (PICT 1548), CONICET (PIP 0674) and UNL (CAI + D 63-91).

References

[1] R.C.T. Slade, J.P. Kizewski, S.D. Poynton, R. Zeng, J.R. Varcoe, in: K.D. Kreuer (Ed.), Fuel Cells: Selected Entries from the Encyclopedia of Sustainability Science and Technology, Springer, New York 2013, pp. 9–29.
[2] J.A. Harrison, Z.A. Khan, J. Electroanal. Chem. 30 (1971) 327–330.
[3] V.S. Bagotzky, N.V. Osetrova, J. Electroanal. Chem. 43 (1973) 233–249.
[4] G. Couturier, D.W. Kirk, S. Srinivasan, Electrochim. Acta 32 (1987) 995–1005.
[5] T.J. Schmidt, P.N. Ross Jr., N.M. Markovic, J. Electroanal. Chem. 524-525 (2002) 252–260.
[6] W. Sheng, M. Myint, J.G. Chen, Y. Yan, Energy Environ. Sci. 6 (2013) 1509–1512.
[7] J. Ohyama, T. Sato, Y. Yamamoto, S. Arai, A. Satsuma, J. Am. Chem. Soc. 135 (2013) 8016–8021.
[8] M.A. Montero, M.R. Gennero de Chialvo, A.C. Chialvo, J. Power Sources 283 (2015) 181–186.
[9] M.R. Gennero de Chialvo, A.C. Chialvo, Phys. Chem. Chem. Phys. 6 (2004) 4009–4017.
[10] P.M. Quaino, M.R. Gennero de Chialvo, A.C. Chialvo, Electrochim. Acta 52 (2007) 7396–7403.
[11] M.A. Montero, J.L. Fernández, M.R. Gennero de Chialvo, A.C. Chialvo, J. Power Sources 254 (2014) 218–223.
[12] M.A. Montero, J.L. Fernández, M.R. Gennero de Chialvo, A.C. Chialvo, J. Phys. Chem. C117 (2013) 25269–25275.
[13] J. Augustynski, M. Koudelka, J. Sanchez, B.E. Conway, J. Electroanal. Chem. 160 (1984) 233–248.
[14] S. Thanawala, D.G. Georgiev, R.J. Baird, G. Auner, Thin Solid Films 515 (2007) 7059–7065.
[15] J.C. Fuggle, N. Martensson, J. Electron Spectrosc, Relat. Phenom. 21 (1980) 275–281.
[16] M.M. Jaksic, B. Johansen, R. Tunold, Int. J. Hydrog. Energy 19 (1994) 321–335.
[17] N.M. Markovic, S.T. Sarraf, H.A. Gasteiger, P.N. Ross Jr., J. Chem. Soc. Faraday Trans. 92 (1996) 3719–3725.
[18] D.M. Drazic, A.V. Tripkovic, K.D. Popovic, J.D. Lovic, J. Electroanal. Chem. 466 (1999) 155–164.
[19] M.S. Rau, M.R. Gennero de Chialvo, A.C. Chialvo, Electrochim. Acta 55 (2010) 5014–5018.
[20] M.S. Rau, M.R. Gennero de Chialvo, A.C. Chialvo, J. Power Sources 229 (2013) 210–215.
[21] E.G. Lewars, Computational Chemistry: Introduction to the theory and applications of molecular and quantum mechanics, 2nd. ed. Springer, New York, 2011 (Ch. 2).